HHS Public Access

Author manuscript

Adv Funct Mater. Author manuscript; available in PMC 2019 March 21.

Published in final edited form as:

Adv Funct Mater. 2018 March 21; 28(12): . doi:10.1002/adfm.201703988.

Electrically Controlled Neurochemical Release from Dual-Layer Conducting Polymer Films for Precise Modulation of Neural Network Activity in Rat Barrel Cortex

Dr. Zhanhong Jeff Du,

Department of Bioengineering, University of Pittsburgh, 5057 Biomedical Science Tower 3, 3501 Fifth Avenue, Pittsburgh, PA 15260, USA

Shenzhen Key Lab of Neuropsychiatric Modulation, CAS Center for Excellence in Brain Science, Shenzhen Institutes of Advanced Technology, Chinese Academy of Sciences, Shenzhen 518055, China

Prof. Guo-Qiang Bi, and

Hefei National Laboratory for Physical Sciences at the Microscale, CAS Center for Excellence in Brain Science and Intelligence, Technology and School of Life Sciences, University of Science and Technology of China, Hefei, Anhui 230026, China

Prof. Xinyan Tracy Cui

Department of Bioengineering, University of Pittsburgh, 5057 Biomedical Science Tower 3, 3501 Fifth Avenue, Pittsburgh, PA 15260, USA

Abstract

Implantable microelectrode arrays (MEAs) are important tools for investigating functional neural circuits and treating neurological diseases. Precise modulation of neural activity may be achieved by controlled delivery of neurochemicals directly from coatings on MEA electrode sites. In this study, a novel dual-layer conductive polymer/acid functionalized carbon nanotube (fCNT) microelectrode coating is developed to better facilitate the loading and controlled delivery of the neurochemical 6,7-dinitroquinoxaline-2,3-dione (DNQX). The base layer coating is consisted of poly(3,4-ethylenedioxythiophene/fCNT and the top layer is consisted of polypyrrole/fCNT/DNQX. The dual-layer coating is capable of both loading and electrically releasing DNQX and the release dynamic is characterized with fluorescence microscopy and mathematical modeling. In vivo DNQX release is demonstrated in rat somatosensory cortex. Sensory-evoked neural activity is immediately (<1s) and locally (<446 μm) suppressed by electrically triggered DNQX release. Furthermore, a single DNQX-loaded, dual-layer coating is capable of inducing effective neural inhibition for at least 26 times without observable degradation in efficacy. Incorporation of the novel drug releasing coating onto individual MEA electrodes offers many advantages over alternative methods by increasing spatial-temporal precision and improving drug selection flexibility without increasing the device's size.

Correspondence to: Xinyan Tracy Cui.

Conflict of Interest

The authors declare no conflict of interest.

Keywords

conducting polymers; controlled neurochemical release; electrochemistry; electrophysiology; neural networks

1. Introduction

Implantable microelectrode arrays (MEAs) directly interfacing neural tissue by stimulation or recording have demonstrated great potential in restoring or bypassing lost neurological function.[1] MEAs can also be used to study neural circuitry dynamics and functional connectivity. For these studies, it is often desired to be able to apply pharmacological perturbations to a small cell population.[2] For example, simultaneous electrophysiological recording from somatosensory cortex while antagonizing individual glutamate receptors has been critical to understanding glutamate receptor contribution during whisker sensation.[3] Pressurized injection,[4] microiontophoresis,[2g,h,3,5] and microfluidics devices[6] have been previously developed to precisely control the local delivery of chemicals into the surrounding environment, including neuronal tissue. These techniques require additional hardware, such as pumps, valves, and fluidic channels, and additionally are subject to drug leakage or tip clogging. In addition, incorporation of fluidic channels onto an MEA increases the overall device size and fabrication complexity. Optogenetic stimulation techniques allow for the modulation of a subpopulation of genetically modified neurons with high precision,[7] but the presence of a fiber-optic cable for optogenetic stimulation increases the device's footprint. Furthermore, optogenetic techniques require genetic modifications.

Conducting polymer coatings can improve neural electrode performance by decreasing electrode impedance, increasing charge injection limits, and promoting neuron adhesion.[8] Further, conductive polymers can be doped with bioactive molecules that can be released with high spatial and temporal fidelity through electrical stimulation.[9] These polymers can be electropolymerized onto any electrode surface, resulting in a positively charged polymer backbone bound with negatively charged dopants. As such, the application of a sufficiently negative current may reduce the polymer backbone and release the dopants. Various biochemically active reagents, such as salicylate, adenosine triphosphate (ATP), 2-ethylhexylphosphate, naproxen, glutamate,[10] and dexamethasone[9p,11] have been electrically released from conducting polymer surfaces based on this mechanism.

We have shown previously electrically triggered release of the 2-amino-3-(5-methyl-3-oxo-1,2-oxazol-4-yl)propanoic acid (AMPA) receptor antagonist 6-cyano-7-nitroquinoxaline-2,3-dione (CNQX) from polypyrrole coatings can transiently inhibit activity of cultured hippocampal neurons.[12] The fast excitatory transmission mediated by the AMPA receptor directly impacts neural network activity due to its involvement in action potential generation.[13] In this study, we further develop this technique for in vivo release of AMPA antagonist. 6,7-Dinitroquinoxaline-2,3-dione (DNQX) was selected to replace CNQX due to its higher water solubility.[14] Both CNQX and DNQX were initially found to be poor dopants that result in an overall decrease of electrical conductivity. This had the effect of limiting polymer growth and minimizing the drug loading capacity.

The incorporation of acid functionalized carbon nanotubes (fCNT) into polypyrrole (PPy) [15] and poly(3,4-ethylenedioxythiophene (PEDOT)[8a,16,17] films can improve electrical conductivity and mechanical stability of the conducting polymer films.[8a,16] Furthermore, the inner cavities of the fCNTs may serve as a nanoreservoir for the incorporation of high concentrations of drug molecules for controlled delivery. This is clearly displayed by the capability of PPy/fCNT films to significantly increase dexamethasone loading and release capacity.[15d] However, even with the incorporation of fCNTs, the impedance of the PPy/fCNT is still increased upon drug loading and the film growth is limited. In this study, we overcome these challenges through the development of a dual-layer electrode coating approach. A previous study used a dual-layer polymer, consisting of an ATP-loaded PPy inner layer and a poly(*N*-methylpyrrole) outer layer, to release ATP.[18] In that case the outer layer was incorporated to improve biocompatibility and to adjust the release profile. In this report, we detail the development of a novel dual-layer approach (see Figure 1a), consisting of a PEDOT/fCNT inner layer designed to maximize conductive surface area and a PPy/fCNT/DNQX outer layer designed to maximize the drug loading capacity.

The in vivo performance of the drug delivery system was evaluated by implanting the dual-layer polymer-coated MEAs into the rat barrel cortex. An air-puff multiwhisker stimulator was used to elicit strong and repeatable neuronal firing in the barrel cortex.[19] This reproducible stimulation was used to characterize the effects of electrically triggered DNQX release on the sensory-evoked neural response. Acute neural recording demonstrated that the sensory-evoked neural network activity in rat primary somatosensory cortex was immediately inhibited by the release of DNQX. The overall effectiveness as well as the temporal and spatial resolution of this novel drug release technique is evaluated in this study.

2. Results and Discussion

2.1. Fabrication and Characterization of the Dual-Layer Coating on In Vitro MEAs

2.1.1. Fabrication of the Dual-Layer Film—For material characterization and drug release quantification, we designed in vitro MEAs with 125 μm diameter Pt/Ir wires embedded in epoxy. The polished cross section of the microwires served as electrode sites with a circular site area of 12272 μm^2. These electrodes are easy to fabricate and are fully reusable by polishing (demonstrated in Figure 1b). This MEA mimics the geometric and electrochemical features of in vivo electrodes (as compared to previously used macroelectrodes with a size area of 0.7–1.54 cm^2).[9a,b,p]

The incorporation of dopants such as DNQX or fluorescein into the PPy film resulted in high-resistance coatings, as demonstrated by the sharply decreased chronoamperometry electrodeposition current (Figure 1d, single-layer drug loading group is in green). The high resistance prevented the film from growing, and thus limited drug loading. To create an electrode surface permissive for thick PPy/fCNT/drug film growth, a layer of PEDOT/fCNT was first deposited on the electrode (Figure 1d). PEDOT/fCNT significantly decreased impedance (Figure 2d) due to the expanded surface nanoscale features, shown in SEM (Figure 2a), as well as the excellent electrical conductivity of PEDOT and fCNT. The most prominent impedance decrease occurs between 10 and 1000 Hz (Figure 2d), which covers the frequency for drug release (10 Hz) and in vivo recording (1000 Hz). Impedance at 1000

Hz is considered to be most relevant for neural spike recording as it matches the time scale of action potentials.[20] The frequency of 10 Hz is relevant to drug release because it corresponds to the time scale of our 100 ms cosine wave drug delivery stimulus (Figure 7d). The PEDOT/fCNT coating was uniform and did not grow beyond the borders of Pt/Ir electrode sites (Figure 1b,c). The initial PEDOT/fCNT layer facilitated the deposition of the second PPy/fCNT/drug layer. The deposition current of the second layer shows a clear increase after the capacitive current and becomes steady but consistently higher than the single-layer current (Figure 1d, double-layer coating is in red). Overall, the dual-layer deposition charge increased ≈40-fold from that of the single layer, indicating that the initial PEDOT/fCNT layer facilitated the deposition of PPy/fCNT/drug. For the second layer, PPy was chosen over PEDOT for two reasons. First, in our experience PPy showed significantly higher redox current and more drug release than PEDOT when electropolymerized under the same conditions and with the same drug molecule. Second, the reduction potential of PPy is around −0.34 V,[9p] which is lower in magnitude than the reduction potential of PEDOT (−0.7 V).[21] −0.7 V exceeds the previously defined safety window of −0.6 to 0.8 V for electrical stimulation, at which water hydrolysis and other electrochemical reactions may harm tissue.[22,23]

2.1.2. Characterization of the Dual-Layer Film—PEDOT/fCNT polymerizes into a porous and fibrous 3D matrix (SEM imaging shown in Figure 2a). This matrix results in a highly conductive surface area for PPy/fCNT/drug film growth.

Qualitatively, the deposition of the second PPy/fCNT/fluorescein layer increased nanofiber diameter as compared to PEDOT/fCNT, but the overall nanoporous and fibrous morphology did not change significantly (Figure 2b). Thus, the surface area for drug release is very large and the hollow area between fibers would allow for drug loaded in the deeper portions of the matrix to be released. Another benefit of fCNTs is that they can be used as a nanoreservoir to replenish the drug load at the outer surface of the polymer.[15d] The fCNTs used in this study have an outer diameter between 10 and 20 nm and an inner diameter between 5 and 10 nm. The inner/outer diameter ratio is larger than that of the fCNTs used in our previous study detailing the controlled electrical release of dexamethasone.[15d] This increased ratio is expected to offer more internal space for drug loading.

Cyclic voltammetry (CV) measurement of the single-layer and dual-layer PPy/fCNT/fluorescein films also revealed very different characteristics (Figure 2c). The dual-layer film exhibits a larger current, with a prominent reduction peak around −0.45 V. The charge storage capacity (CSC) of the bilayer is 8.8× higher than that of the single-layer film. Furthermore, the impedance of the double-layer polymer at 10 Hz, the frequency relevant to drug release, is almost 10 times lower than the single-layer polymer, greatly increasing the Faradaic efficiency of drug release.

2.2. Drug Release Quantification

2.2.1. Microscopic Semiquantitative Analysis of Fluorescein Release—It is difficult to obtain an accurate measurement of the amount of drug released from drug-loaded microelectrode upon electrical stimulation due to the small absolute quantity of drug evoked.

Previously, high surface area macroelectrodes were used to quantify drug release because the release quantity could be directly measured. However, we have found that the drug release profile from macroelectrodes does not accurately model drug release from microelectrodes. First, electrodeposition of conducting polymer does not produce uniform coating on macroelectrodes, while polymer coatings are commonly more uniformly distributed on microelectrodes. Second, the charge injection is more efficient at microelectrodes (higher charge density), which results in more efficient stimulated release. With these considerations, it is highly important to develop a method to assess drug release from microelectrodes. We have addressed this issue by developing a method that incorporates fluorescein into the dual-layer coating as a model molecule to mimic DNQX release dynamics at microelectrodes in vitro. While direct measurement of DNQX is impossible due to the small quantity, fluorescent imaging and quantification of fluorescein is readily attainable. The selection of fluorescein to mimic neurochemical DNQX was appropriate because both molecules have two net charges in their disodium salt form, both are similar molecular weights (332 and 252 g mol^{-1}, respectively) and both exhibit good water solubility.

Fluorescence microscopy was used to image fluorescein release upon electrical stimulation. The amount of fluorescein released was quantified based on fluorescence intensity. The timing paradigm (Figure 3a) and imaging setup (Figure 3b) are detailed in Section 4. An initial cosine waveform (−1.5 V, 100 ms) was utilized to trigger drug release. This was immediately followed by a second cosine waveform (0.75 V, 200 ms) delivered to balance the charge. This waveform is the same as the in vivo stimulus waveform shown in Figure 7d. The fluorescent intensity was highest immediately after the drug release trigger (Figure 3c,d, trigger marked by the red vertical line) and gradually decreased as the dissociated drug diffused away from the probe. Fluorescein quantity is considered to be linearly related to the change in fluorescence intensity (obtained by subtracting baseline fluorescence intensity from the maximum intensity).

This semiquantitative measurement of fluorescein release was repeated for stimulus amplitudes of 1, 1.5, and 2 V. The drug release at 1 V is significantly lower than 1.5 and 2 V (Figure 3e), indicating that the amount of reduction reaction triggered by each stimulation amplitude is not linearly related to the voltage.

Toward generating a mathematical model of the drug release profile from microelectrodes, two phases of the drug delivery process were noted and combined. In the first phase, the quantity of releasable drug is limited but the time for the drug to exit the film is short, thus this phase of release fits a faster decay exponential with a larger initial value. Because of the rapid release, the drug molecules are not likely to be drawn back to the film by the anodic current in the second charge balance phase of the stimulus. The second phase is the replenishment of drug from the inner film reservoir, which can be described by a slower decay exponential due to the large volume of the reservoirs and lower mobility of the drug in the film. Consequently, the release amount after sufficient trials almost reaches a steady state, when surface release rate and internal replenish rate are roughly equal. Based on this justification, Equation (1) was developed as the summation of two exponential decays to fit the experimental data. The fit quality was very good for the 1, 1.5, and 2 V release groups

(Figure 4a–c, R^2 between 0.994 and 0.996), indicating that the model captures the important physical properties of this controlled release process. For Equation (1), A is the constant used to determine the general range of fluorescent intensity for each dynamic, C is the ratio of the second mechanism compared to the first mechanism in determining the final outcome, B and D are the constants used to determine the rate of each decay process, and x is the release number from 1 to 90. The fitting parameters as well as the coefficient of determination R^2 are listed in Table 1. It should be noted that because the 1 V release was too weak, the decay trend for the second mechanism was too weak. Thus, parameters C and D could not be accurately estimated for the 1 V release

$$C_{\text{Fluo}} = A * e^{B*x} + C * e^{D*x} \quad (1)$$

The observed quantities of fluorescein for release volleys 1–5 were drastically variable, especially for 1.5 and 2 V. This is partially caused by the random quantity of physically adsorbed drug molecules on each electrode after phosphate buffer solution (PBS) washing. The random adsorption of drug molecules may reflect the random nanosurface formed on the outermost layer of polymer. Thus, release volleys 1–5 were removed from all model fitting. A small peak was initially observed following 1.5 and 2 V stimulation. This is possibly due to a lower concentration of fluorescein in the superficial layer as compared to deeper regions. This is likely due to the PBS washes and is overcome by replenishment with drug from the reservoir. The model clearly predicts that the quantity of each drug release heavily depends on the previous release history as well as the amplitude of stimulus current. Because parameters A, B, C, and D all depend on the release trigger amplitude, it is possible to adjust the amplitude to obtain more or less release quantity according to the experimental need. By carefully tuning the release amplitude, e.g., using smaller amplitude in early trials but larger amplitude in later trials, it is possible to maintain a constant dose of drug release per trigger for many trials. This would be highly desired for both neuroscience research and therapeutic applications.

2.2.2. Spectrometry and Mathematical Modeling of Drug Release—To further estimate the absolute quantity of release, accumulative release with the 1.5 V 100 ms cosine trigger was measured using spectrometry. The UV absorption detection limit of DNQX is 0.16×10^{-6} M while the detection limit of fluorescein based on emission can be as low as 0.44×10^{-9} M. Due to the difficulty to measure DNQX release from a microelectrode with a single trigger, released drug pooled from multiple stimulation volleys was used for the quantification of fluorescein and DNQX (cumulative release). Even with the cumulative drug release, the quantity of DNQX is still too small for detection. Thus, an ultrasmall volume drug release system is designed with a release solution volume of 60 μL and a sample volume of 50 μL (Figure 4d) to maximize drug concentration. The cumulative release of fluorescein in this small volume for release volleys 1–45 and 4–90 is illustrated in Figure 4e. Using the model established in Equation (1) and the release quantity from release volleys 1–45, the predicted release quantity from release volleys 46–90 is 0.49 μg cm^{-2}. This is in good agreement with the measured release (0.49 ± 0.07 μg cm^{-2}), which provides validation for the model. The spectroscopy quantification of DNQX cumulative release 1–45

was utilized to calculate the model-predicted cumulative DNQX of release volleys 46–90 (Figure 4f) in order to test the hypothesis that fluorescein and DNQX follow the same release trend. The model prediction of 47.17 μg cm^{-2} for DNQX is also in good agreement with the measured DNQX release for 46–90, 56.45 ± 13.62 μg cm^{-2}, thus indicating that the model captures the release dynamics of DNQX. Accounting for the electrode size of MEAs used in vivo, we can estimate that the quantity of each individual DNQX release in vivo is in the range of 15.7 pg (release 90) to 115.1 pg (release 8).

The cumulative releases of DNQX and fluorescein both agree with the model prediction, suggesting that the two molecules share similar release dynamics. It is important to note however that despite the similarity between fluorescein and DNQX in the ratio of release volleys 1–45 and 46–90, the absolute release quantity per area is very different. The electrode can deliver fluorescein up to 0.04 μg cm^{-2} and DNQX up to 4.09 μg cm^{-2} with the 100 ms 1.5 V amplitude cosine waveform. This indicates that the polymer may display similar release trend with the same trigger type, with the release quantity heavily depending on the nature of the dopant itself.

2.3. In vivo Neural Network Activity Modulation

2.3.1. Electrochemical Deposition and Characterization of the Bilayer Drug-Release Coating on In Vivo MEAs—To test the effectiveness of the drug release system in vivo, commercial Neuronexus probes were utilized. Individual microelectrodes were selectively coated with the bilayer films, with the first layer being PEDOT/fCNT and the second layer being PPy/fCNT/DNQX (Figure 5a). The coating is contained to the border of the iridium microelectrode area (Figure 5b). In Figure 5b,c, electrode sites 14 and 11 are coated with dual-layer PPy/fCNT/DNQX. The pre- and postsurgery images of sites 14 and 11 show that the polymer morphology remains the same after surgery, which indicates that the polymer coating is sufficiently strong and adherent to survive the insertion and multiple electrically triggered drug releases and explanation with no sign of cracking or delamination on microscopic scale. The electrodeposition of PPy/fCNT/DNQX (Figure 6a) onto PEDOT/fCNT demonstrated much larger initial current and total integrated charge than those onto bare metal electrode sites (single layer). This is consistent with the trend observed for in vitro MEAs.

The 1 kHz impedance (Figure 6b) of single-layer PPy/fCNT/DNQX microelectrodes is above 1 MΩ, making it difficult to record low-noise high-quality neural signal. Nonetheless, PEDOT/fCNT base layer coating reduced the 1 kHz impedance to ≈20 kΩ, and the deposition of PPy/fCNT/DNQX on top of it resulted in a final impedance of 450 kΩ, well within the impedance range suitable for high-quality neural recording from this type of MEAs.

As is the case of in vitro MEAs with fluorescein containing coatings, CV experiments reveal that the CSC of dual-layer DNQX coating (168 mC cm^{-2}) is also much higher than that of the single-layer coating (32 mC cm^{-2}) on in vivo MEAs (Figure 6c). The redox potential of DNQX-loaded PPy/fCNT films was similar to the fluorescein-loaded films polymerized on the in vitro MEAs (Figure 2c), but the CSCs are much higher than that of the fluorescein films on the in vitro MEAs (49 mC cm^{-2}).

2.3.2. DNQX Releases Effectively Suppressed Sensory-Evoked Neural Activity in Rat Barrel Cortex—To test the in vivo effectiveness of the drug release MEA, coated MEAs were implanted into barrel cortex of rats and evoked neural activity upon whisker stimulation was recorded (Figure 7a). A simultaneous recording and whisker stimulation setup with isolated counterelectrodes was utilized to lower electrical artifacts from stimulation.[24] Figure 7d illustrates the experimental scheme. The first whisker air puff burst (each burst is 100 ms on, 150 ms off with three repeats) began at 0 s, and three consecutive bursts were delivered at 5 s intervals to assess barrel cortex response. DNQX was released at 4 s, 1 s before the second burst. The third burst was delivered to assess the effective duration of the released DNQX. At least one additional minute was allowed before the next drug release trial so that barrel cortex fully recovers from previous DNQX release. Because a single electrode site is too small to release sufficient drug to affect neural activity, four drug-loaded electrodes (Channels 7, 8 14, and 11 as seen in red in Figure 5a) were stimulated simultaneously for each release to provide maximum drug effect. The raw neural signal filtered between 300 and 3000 Hz was used for extracting extracellular action potentials. During each burst of air puff stimulation, a high firing rate was observed during the 100 ms period when air puff was on, and relatively low firing rate was observed during the 150 ms air-puff off period (Figure 8a). The peak-to-peak noise recorded from recording electrodes was roughly 15 μV and a large quantity of multiunit spikes was detected from the raw data. The artifact of drug release trigger was transient due to careful isolation of the circuits with the respective counterelectrodes placed far from each other (as shown in Figure 7a). The drug release effect was clearly observable (Figure 8a, middle panel) when compared to control activity (Figure 8a, upper panel). The spike number during the air puff and interval were all decreased due to DNQX release. This is an expected effect of DNQX, as it effectively blocks the AMPA-receptor-mediated glutamate transmission which is essential for action potential generation.

The spike generation begins to recover ≈1 s following drug release (Figure 8a, middle panel, green circle). 6 s following the release trigger, the drug effect was almost completely washed away (Figure 8a, lower panel). This in vivo DNQX clearing rate is much faster than the in vitro condition where CNQX release was still very effective 7.5 s after drug release.[12]

The firing pattern of the recorded channel was further analyzed by calculating the sensory-evoked raster plot (Figure 8b) and peristimulus time histogram (PSTH; Figure 8c). In the raster plot each black or red small vertical line indicates an action potential: black denotes the control trials and red denotes the DNQX release trials. The air puff on and off are emphasized by red and blue semitransparent boxes, respectively, in Figure 8b. During the control trials, the relative timing of evoked spikes after air puff was very reliable. In contrast, during release trials, the number of spikes was reduced for each air puff and almost completely suppressed after drug release.

The PSTH of a representative recording channel was calculated to perform an effective analysis on the change in the rate of evoked action potentials (Figure 8c). Each sensory stimulus evoked a strong and instantaneous firing rate increase, but due to neuron adaptation, the amplitude of the firing rate decreased from first to third air puff. During these “on” periods, the drug release significantly reduced the firing rate with the effect being the

strongest in the third period. Due to the nonlinear response properties of neurons, the spike number is very small and is sensitive to input level change when the input is weak. When the input is strong, the spike number is high and less variable. DNQX inhibits AMPA receptors and thus reduces the input strength of postsynaptic neurons. The phenomenon that weaker sensory responses are suppressed more but stronger responses are less affected indicates that the mechanism of firing rate reduction is indeed a result of released DNQX. Additionally, considerable neural activity was observed during the off period (blue semitransparent box) in the control, while these activities were nearly abolished after the DNQX release, and the oscillatory firing rate increase in control cannot be observed during the DNQX inhibited trials. This oscillatory firing rate increase could be the residual vibration of the rat whisker, thus this may assimilate the natural sensing process more closely than strong artificial air puffs to the whisker. The most prominent effect of DNQX release is the abolishment of the increase in oscillatory firing rate (blue box). Thus, it is possible that this technique can efficiently block rat facial whisker sensing while the animal is awake and behaving.

The sensory-evoked spike number on each channel was aggregated and normalized to baseline-evoked spike number on the same channel before and after DNQX release effect to further analyze the in vivo reproducibility of the drug release film as well as the distance of the drug release effect. The DNQX effect of one release volley was observed for 90 s until the next drug release trigger was delivered. Eight recording electrodes positioned near the four drug releasing electrodes (Figure 5a) were utilized to characterize the effectiveness of drug delivery.

The normalized spike number decreased after DNQX release was averaged across the eight recording channels (Figure 8d). The normalization yields 1 when the DNQX effect is completely unobservable and 0 when all spikes are suppressed by DNQX release. The effect of DNQX release was still observable after 26 consecutive release trials. Furthermore, the drug effect was very strong and stable across the 26 trials. Further trials were not pursued due to deteriorating baseline physiological firing rate after long periods of anesthesia. The in vitro quantification in Figure 4f indicates that DNQX can be released up to 90 times, and that the DNQX release quantity from four electrodes is between 15.72 and 115.14 pg until release 90. Therefore, based on the in vitro characterization we expect that drug release effectiveness is likely to last much longer than the 26 observed trials in vivo. It is possible to characterize the technique with other animal models or with anesthesia strategies designed for better physiological baseline stability.

The normalized spike number change on each channel was averaged across the 26 trials and plotted against their distance from site 10 (Figure 8e) to estimate the effective distance of drug release. The geometric center of four drug release sites 7, 8, 14, and 11 colocalizes with channel 10, therefore the highest drug concentration should be at channel 10. A clear decay of drug release effectiveness was observed (Figure 8e), with faster decay near the center of drug release. Thus, a Gaussian function in Equation (2) was utilized to fit the trend for drug release effectiveness $\mathrm{Eff}_{\mathrm{Drug}}$ against distance x. Because the peak effect of drug release is always in the center, the constant c of Gaussian function which determines the center shift is fixed at 0 μm. The constant a represents the peak effectiveness of drug release and b represents the spatial extent of drug effect. The fit to Equation (2) was excellent, with a

goodness of fitting $R^2 = 0.985$. The constants were determined to be $a = 0.83$, $b = 223$. According to the fit, the drug effect at 223 μm was half of the peak effect in the center and the effect almost completely faded at 446 μm (effect reduced to ≈13.5% at 2σ from the center of the Gaussian function). Based on the above results, it can be concluded that electrically triggered release of DNQX was most effective at suppressing neural activity for 6 s and within a 446 μm zone. Furthermore, the effect is reversible. The neural activity recovers completely following drug release

$$\mathrm{Eff}_{\mathrm{Drug}} = a * \mathrm{e}^{-\frac{x^2}{2*b^2}} \quad (2)$$

Following 6 h of in vivo experimentation, the MEAs were explanted and dipped in trypsin to remove any tissue on the surface. There was no observable damage to the coatings after in vivo use (Figure 5b,c), indicating that the coating is mechanically stable upon insertion and explanation. The mechanical stability of the PEDOT/fCNT layer was further explored in previous studies.[17c] Thus with the strong binding layer of PEDOT/fCNT, the drug loading dual-layer polymer is sufficiently strong to withstand the surgery insertion and in vivo drug release. Furthermore, electrical stimulation caused no degradation to the electrochemical properties of the dual-layer PPy/fCNT/DNQX coating as the retrieved MEAs can still be utilized for neural recordings. In this experimental paradigm, we chose to stimulate four drug-loaded electrodes at the same time to maximize drug release. From our preliminary experiment, the neural activity change from single site release was small. Although increasing amplitude of stimulation may cause more drug release from one single electrode, the chance of damaging tissue or generating electrically induced neuron activation will be greatly increased. Designing electrode arrays with larger drug releasing sites may solve this problem in the future.

Rat barrel cortex serves as an outstanding testbed to evaluate the DNQX release because action potentials can be reliably evoked by stimulating specific facial whiskers in a topographical manner.[25] The cortical input layer IV produces the most reliable and largest number of evoked neuronal firing with low spontaneous activity and low latency.[26] Iontophoresis studies with *N*-methyl-D-aspartate and AMPA receptor blockers in the barrel cortex successfully elucidated the AMPA receptor function in barrel cortex activity.[3] However, because an iontophoresis device can only be easily combined with single channel recording glass electrodes, this multichannel simultaneous recording and pharmacological intervention tool with electrically controlled release may provide new insight to elucidate the neural network dynamics. In comparison with other pharmacological modulation techniques such as cannular injection and iontophoresis, this novel electrochemically controlled drug release offers much simpler implementation to combine with any MEAs. The technique is more reliable and does not introduce any fluidic movement that would disturb the tissue and inevitably affect neural activity. It also avoids fluidic leaking or channel clogging, and requires no extra devices (such as pumps). Previous studies have used conducting polymers to deliver drugs,[9q] but this work is the first demonstration of using the drug delivery capability of conducting polymers to directly modulate neural network activity in vivo for a

functional neural circuit study. In addition, this study provided indepth analysis of drug delivery quantity from microscale electrodes. Different from prior work, controlled electrical release of DNQX was performed using a novel prolonged cosine waveform with very low rising slope.[24] This waveform was chosen to avoid activating surrounding neurons due to capacitive currents associated with the drug release trigger event, as revealed by theoretical modeling of deep brain stimulation.[27] The elegant work utilizing PEDOT as ion pumps has also shown successful modulation of in vivo neural response.[28] In comparison, the fabrication of such organic ion pump is relatively difficult and requires larger device volume for the delivery channel. The ion pump approach also requires high electrical fields to drive ionic drug out and is not able to deliver larger molecules that has limited diffusion in the long PEDOT channel. Our technology is easily implemented on microelectrode arrays and is more energy efficient. Although large molecules will be more difficult to release due to the high diffusion resistance, these molecules do not need to travel a long distance as in the case of ion pump. Indeed, proteins such as NT3 and BDNF have been previously incorporated in conducting polymer films and released upon electrical stimulation.[9b–d,29] With the incorporation of CNTs, the polymer films become nanofibrous with large open space. Such porous structure may also facilitate the release of large molecules.

Comparing to other novel techniques such as optogenetics and pharmacogenetics, the electrochemically controlled drug release requires no light source or special-designed drug molecules. Also, the technique has much faster test cycles because no virus injection or vector expression is required. This technique can even be combined with optogenetics to achieve both cell type selectivity and receptor selectivity. Since no genetic modification is involved and many drugs are already approved for clinical use, the technique has exceptional potential for clinical translation. Overall, the method provides a unique and powerful tool for basic neuroscience research, and further development may find use in neural modulation devices for therapy.

3. Conclusion

The novel dual-layer coating with PEDOT/fCNT substrate markedly improved the electrodeposition of PPy/fCNT/drug on microelectrodes. The dual-layer polymer demonstrated excellent electrical conductivity and can be electrically triggered to release drug on demand. The mechanical stability of the dual-layer coating was sufficient to withstand the surgery insertion and repeated in vivo drug release triggers. Ultralow concentration semiquantification of fluorescein release was achieved by fluorescent microscopy and a double-exponential decay function successfully captured the trend of drug release concentration at various stimulation amplitudes. The repeated and transient suppression of sensory transmission in barrel cortex indicates that the releasable DNQX amount is sufficient to directly modulate neural network activity in vivo. Interestingly, weaker neural networks are affected more, consistent with the nonlinear response properties of neurons and the DNQX’s function. These results showed great promise of using conducting polymer dual-layer coating for precise release of neurochemicals to modulate neural activity in vivo. Future work will optimize the coating and MEA design for widespread use of the technology in neuroscience research and neural prosthesis applications.

4. Experimental Section

Materials and Chemicals

DNQX disodium salt was acquired from Abcam (MA), and multiwalled carbon nanotubes (CNT) were purchased from Nanoamor (TX) and were chemically functionalized with −COOH using a previously reported method.[15d] In brief, CNTs were sonicated in acid solution (1:3 HNO_3 and H_2SO_4) for 2 h to functionalize the surface and open the CNT ends as well as remove the potentially toxic heavy metal catalyst. Ultracentrifuge (Sorvall RC 6 plus, Thermo Scientific, PA) at 12k–19k rpm was utilized to wash the residual acid until pH reaches neutral. All other chemicals were obtained from Sigma-Aldrich (MO). 16-channel in vivo MEAs were obtained from Neuronexus (MI), with an electrode site area of 703 μm^2. The electrodes are on four shanks with four electrodes on each shank. Electrodes are spaced 100 μm on the same shank and 125 μm between shanks.

In vitro *MEAs* were fabricated with Pt/Ir wires and UV-curing epoxy. Briefly, three wires were carefully aligned inside a 200 μL pipette tip filled with degassed epoxy. The epoxy was cured for 5 min and consolidated for 5 min from the side. The array was cut with a handsaw and polished with alumina particle electrode polishing kit (CH Instruments, Inc., TX), with particle diameters of 1 and 0.3 μm sequentially. During fluorescein release, a black nonfluorescent liquid electrical tape (Mcmaster-Carr, IL) was also applied to the surface of the epoxy array to minimize background light.

Electrochemical Polymerization and Characterization

On both in vitro and in vivo MEAs, PEDOT/fCNT were deposited with a Gamry FAS 2 Femtostat (PA). The deposition solution contained 3,4-Ethylenedioxythiophene (EDOT, 0.015 M) and fCNT(1 mg μL^{-1}) in deionized water (DI H_2O, 1 mL). Sonication by a probe sonicator (Q500, Qsonica, CT) for 15 min homogenized the fCNT and EDOT. A three-electrode cell consisting of a platinum sheet counter and Ag/AgCl reference was utilized, and 0.95 V was applied for 15 s to form the PEDOT/fCNT film. Then, the MEAs were removed from the deposition solution, rinsed with DI H_2O, and dried for 5 min. Fluorescein (13.3×10^{-3} M, 5 mg mL^{-1}) or DNQX (16.9×10^{-3} M) was loaded into fCNT (1 mg mL−1) by 5 min of sonication. Pyrrole monomers (0.45 M) were mixed with fCNT containing drug and further sonicated for 5 min. Chronoamperometry deposition of 0.75 V for 15 s was applied to bare electrodes or PEDOT/fCNT-coated electrode to produce the PPy/fCNT/drug film. The array was washed in stirred PBS for 30 min afterward.

The impedance spectrum between 10 Hz and 32 kHz and CV with a scan rate of 1 V s^{-1} and in the range of −0.9 to 0.6 V were obtained using the Gamry FAS 2 in PBS. For both in vitro and in vivo MEAs, an Ag/AgCl electrode was utilized as reference electrode for EIS measurement, and a platinum sheet as counterelectrode. Images of MEAs were obtained with a Zeiss fluorescent microscope (Germany). SEM images were obtained using a Joel JSM 6330F SEM (Japan). A 5 nm layer of Pd was sputtered onto the electrode to improve the conductivity and 5 kV acceleration voltage was utilized.

In Vitro Quantification of Drug Delivery

The setup for automated semiquantitative characterization of fluorescein release is illustrated in Figure 3b. Dual-layer coated MEAs were mounted onto an electrode holder controlled by a motorized three-axis micromanipulator (Siskiyou Instruments, OR) for fluorescent imaging. A fluorescent microscope (Leica, Germany) with a 488 nm excitation light and a 510 nm emission light was utilized. A Uniblitz shutter was inserted between the lamp and microscope to precisely control the duration of fluorescent excitation light. A solenoid controlled the PBS perfusion and vacuum suction. A Digidata Digitizer (Molecular Devices, CA) generated the cathodic leading cosine waveform with an amplitude of 1, 1.5, and 2 V to trigger the release of fluorescein. The duration of the cosine waveform is 100 ms, followed by a 200 ms, half-amplitude charge balancing phase with reversed polarity. Charge-balanced stimulation prevents tissue damage from net charge injection. A fast charge-coupled device (CCD) camera captures fluorescent intensity at 40 Hz. The synchronization transistor–transistor logic (TTL) signals in the system are generated by Master 8 (AMPI, Israel). The timing schematics of fluorescein release imaging is illustrated in Figure 3a. The PBS perfusion for 15 s is executed at the beginning of each drug delivery trial, ensuring the 5 s baseline fluorescent imaging following perfusion. Then, the fluorescent shutter is turned on and the camera recording starts at the same time. Drug release is triggered 5 s after the camera start to take baseline measurement. Another 10 s of drug release are captured to quantify the fluorescein release and diffusion pattern. The microscope shutter is then turned off and 5 s intertrial interval is used to save the image series. 90 fluorescein release trials were conducted for each bilayer-coated fluorescein microelectrode, to capture the full trend for the drug release dynamics.

The drug release setup for spectrometry quantification of drug delivery is illustrated in Figure 4d. The setup allowed the released drug to be accumulated in a very small volume to obtain the highest concentration for precise spectrometer measurement. A small Petri dish filled with DI H_2O underneath the release electrode served as a moisture chamber to prevent excessive evaporation of drug release solution. The slide and the platinum wire counterelectrodes were positioned in the moisture chamber and 60 μL of PBS is added on top of the slide covering the platinum wire and forming a liquid bubble under surface tension. The fluorescein or DNQX containing electrode is carefully positioned with a helping hand or micromanipulator to be submerged in the liquid bubble without touching counterelectrode or the slide surface. 1.5 V drug release waveform was applied to the electrode for 45 times to replicate the exact same amount of fluorescein release recorded by fluorescent microscope. After the drug release trigger, repetitive pipetting was utilized for gently homogenizing the drug release solution. 50 μL of release solution was then extracted from the liquid bubble and measured in a 96-well plate for the quantification of analytes. During the entire process, evaporation is minimized by a humidity chamber. The quantity of fluorescein or DNQX in this solution is used as the basis to calculate the total fluorescein release in the 60 μL solution. Fluorescence spectrometry with excitation wavelength of 488 nm and emission wavelength of 510 nm was utilized to quantify the amount of released fluorescein in the solution, and UV absorption at 248 nm was utilized to quantify the amount of DNQX in the solution.

Due to the extremely low quantity of fluorescein molecules released by microelectrode during each trial, the 90 trial concentration of fluorescein was pooled into the same solution for cumulative quantification. Trials 1–45 consisted the first release amount and trials 46–90 consisted the second release amount. Despite the extremely small amount of analyte present in the release solution, a measurable concentration of fluorescein or DNQX was obtained.

Animal Surgery and Electrophysiology Recording

All animal work was performed under the guidelines of the University of Pittsburgh Institutional Animal Care and Use Committee (IACUC). Sprague–Dawley rats were anesthetized under isoflurane (3%) and head-fixed in an SR-6R stereotaxic frame (Narishige, NY). Two skull screws were carefully positioned above the right motor cortex and left visual cortex of the rat as illustrated in Figure 7a. A 1 mm × 1 mm window above the barrel cortex of the right hemisphere was created by a motorized drill. The center of barrel cortex coordination was 2.5 mm posterior to Bregma and 5.5 mm lateral to the midline. The dura mater was then recessed with a bent 30 Gauge needle and a spring-loaded microscissors. To prevent the potential toxicity of fCNT and drug molecules being spontaneously released in vivo, the electrodes were washed for 30 min in stirred PBS before implant, so the physically adsorbed drug and fCNT are removed. The neural probe was then inserted into the cortex using a micromanipulator at a slow speed to 900 μm beneath the cortical surface where the layer IV of barrel cortex is located, as demonstrated in Figure 7b. The recording counterwire was tied to skull screw above the ipsilateral motor cortex while the release trigger counter was a skull screw above the contralateral visual cortex to minimize stimulation artifact as shown in Figure 7a.

A portable air compressor with compressed air tank was used to deliver 15 psi air puff stimulation to the rat facial whiskers in Figure 7d. The air puff and drug release trigger timing are synchronized by RX5 recording processor. A piezoelectric sensor and an oscilloscope were utilized to measure the delay in the air puff whisker stimulation system. The air puff system created 20 ms delay in the process of delivering compressed air to the rat facial whiskers and this delay was corrected in the analysis. The recording performance of the implanted MEAs was carefully optimized once the principal whisker (with the maximum number of evoked action potentials) was discovered. A custom-built electrode adapter was utilized to completely segregate the neural recording and electrical stimulation circuit to ensure the safety of neural recording during simultaneous stimulation trials and reduce the stimulation artifact. Multichannel neural stimulation signal to trigger the DNQX release was generated by an MS16 stimulator (TDT, FL) controlled by an RX7 (TDT, FL). The neural signal from MEAs was amplified using a 16-channel Medusa preamplifier and recorded with an RX5 processor at 25 kHz (TDT, FL). Neural signal was imported into MATLAB with custom scripts. The synchronization of neural recording, drug release trigger, and whisker air puff was controlled by RX 5 and RX 7 units. Contralateral air puff nozzle was made of a flat-end needle. The nozzle was carefully positioned around 1 cm above the top row of whiskers with a helping hand and repetitive air puff stimulations was delivered to confirm the principal whisker of the barrel that the neural electrode array was implanted. The air puff stimulator reliably evoked strong neural activity in the layer IV of barrel cortex. Each air puff stimulation to the whisker lasts 100 ms in duration and was delivered at 4 Hz to evoke

strong neural response. Once the principal whisker for the implant's location was determined, the electrode depth was slowly adjusted for maximizing sensory-evoked firing rate. The probe is located at the depth in layer IV to evoke the strongest sensory response from the principal whisker.

A cosine waveform with amplitude of −3 μA and duration of 100 ms was delivered to each microelectrode to trigger the release of DNQX, as illustrated in Figure 7c. The drug release current is followed by a reverse phase current with 1.5 μA amplitude and 200 ms duration to balance the change. The charge balance phase serves two functionalities: reduces the net charge delivered to local tissue in order to maintain the safety of the neurons adjacent to the probe and partially reverses the reduction of PPy polymer so that the conjugated polymer maintains sufficient conductivity for the next drug release triggers. In Figure 7d, the air puff stimulation to the whiskers is delivered in burst of three air puffs. The intensity of each burst of air puff is sufficient to quantify the effectiveness of released DNQX molecules.

Data Analysis

The raw data stream was imported into MATLAB and processed with custom scripts. The spike data stream was bandpassed between 300 and 3000 Hz because the typical waveform of extracellular action potentials is roughly 1000 Hz. After the filtering process, a common average reference technique was applied to recordable sites, to remove stimulation artifacts and waveform deviation caused by the reference electrode. The standard deviation (SD) of the spike data stream was calculated, and 3 × SD was utilized to threshold the waveforms. All threshold crossing waveforms with 0.4 ms before and 0.8 ms after the threshold crossing time point were utilized as multiunit recording waveforms to calculate the firing rate and the drug release effect of the system. 20 ms window was utilized to calculate the PSTH of the sensory stimuli.

Acknowledgments

The authors acknowledge the financial support by NIHR01NS062019, 7R43DA035545-02, 1R43DA036264-01, 1R43AA022030-01, and R01NS089688, the National Science Foundation (NSF) Grant ERC-0812348, and the Shenzhen Governmental Basic Research Grants JCYJ20160531174444711 and LSGG20160428140402911. The authors thank the Center for Biological Imaging at the University of Pittsburgh and Dr. Simon Watkins, regarding the use of the facility to perform image analysis. The authors would also like to thank Dr. Daniel J. Simons for advices on barrel cortex recording paradigm and James Eles and Dr. I. Mitch Taylor for editing and proofreading this manuscript.

References

1. a) Wolpaw JR, Birbaumer N, McFarland DJ, Pfurtscheller G, Vaughan TM. Clin. Neurophysiol. 2002; 113:767. [PubMed: 12048038] b) Kozai TD, Du Z, Gugel ZV, Smith MA, Chase SM, Bodily LM, Caparosa EM, Friedlander RM, Cui XT. J. Neurosci. Methods. 2014; 242C:15.c) Motta PS, Judy JW. IEEE Trans. Biomed. Eng. 2005; 52:923. [PubMed: 15887542]
2. a) Tzschentke T. Prog. Neurobiol. 2001; 63:241. [PubMed: 11115727] b) Kandler K, Katz LC, Kauer JA. Nat. Neurosci. 1998; 1:119. [PubMed: 10195126] c) Maalouf M, Dykes R, Miasnikov A. Brain Res. 1998; 793:149. [PubMed: 9630587] d) Lesniak MS, Upadhyay U, Goodwin R, Tyler B, Brem H. Anticancer Res. 2005; 25:3825. [PubMed: 16312042] e) Hyland B, Reynolds J, Hay J, Perk C, Miller R. Neuroscience. 2002; 114:475. [PubMed: 12204216] f) Sawaguchi T, Goldman-Rakic PS. J. Neurophysiol. 1994; 71:515. [PubMed: 7909839] g) Williams GV, Rao SG, Goldman-Rakic PS. J. Neurosci. 2002; 22:2843. [PubMed: 11923449] h) Williams GV, Goldman-Rakic PS.

Nature. 1995; 376:572. [PubMed: 7637804] i) Rao SG, Williams GV, Goldman-Rakic PS. J. Neurosci. 2000; 20:485. [PubMed: 10627624] j) Sawaguchi T, Goldman-Rakic PS. Science. 1991; 251:947. [PubMed: 1825731]

3. Armstrong-James M, Welker E, Callahan CA. J. Neurosci. 1993; 13:2149. [PubMed: 8097531]
4. a) Barker M, Billups B, Hamann M. J. Neurosci. Methods. 2009; 177:273. [PubMed: 19014970] b) Gerhardt GA, Palmer MR. J. Neurosci. Methods. 1987; 22:147. [PubMed: 3437777] c) Tamamaki N, Nojyo Y. Hippocampus. 1993; 3:471. [PubMed: 8269038]
5. Hicks TP. Prog. Neurobiol. 1984; 22:185. [PubMed: 6089267]
6. a) Mourzina Y, Kaliaguine D, Schulte P, Offenhäusser A. Anal. Chim. Acta. 2006; 575:281. [PubMed: 17723603] b) Kaji H, Nishizawa M, Matsue T. Lab Chip. 2003; 3:208. [PubMed: 15100776]
7. a) Nagel G, Szellas T, Huhn W, Kateriya S, Adeishvili N, Berthold P, Ollig D, Hegemann P, Bamberg E. Proc. Natl. Acad. Sci. USA. 2003; 100:13940. [PubMed: 14615590] b) Cardin JA, Carlen M, Meletis K, Knoblich U, Zhang F, Deisseroth K, Tsai LH, Moore CI. Nature. 2009; 459:663. [PubMed: 19396156] c) Zhang F, Wang LP, Brauner M, Liewald JF, Kay K, Watzke N, Wood PG, Bamberg E, Nagel G, Gottschalk A, Deisseroth K. Nature. 2007; 446:633. [PubMed: 17410168] d) Sohal VS, Zhang F, Yizhar O, Deisseroth K. Nature. 2009; 459:698. [PubMed: 19396159] e) Boyden ES, Zhang F, Bamberg E, Nagel G, Deisseroth K. Nat. Neurosci. 2005; 8:1263. [PubMed: 16116447] f) Anikeeva P, Andalman AS, Witten I, Warden M, Goshen I, Grosenick L, Gunaydin LA, Frank LM, Deisseroth K. Nat. Neurosci. 2012; 15:163.g) Lu Y, Li Y, Pan J, Wei P, Liu N, Wu B, Cheng J, Lu C, Wang L. Biomaterials. 2012; 33:378. [PubMed: 22018384]
8. a) Kozai TDY, Catt K, Du Z, Na K, Srivannavit O, Haque R-uM, Seymour J, Wise KD, Yoon E, Cui XT. IEEE Trans. Biomed. Eng. 2016; 63:111. [PubMed: 26087481] b) Du ZJ, Luo X, Weaver CL, Cui XT. J. Mater. Chem. C. 2015; 3:6515.
9. a) Thompson BC, Moulton SE, Richardson RT, Wallace GG. Biomaterials. 2011; 32:3822. [PubMed: 21353699] b) Thompson BC, Moulton SE, Ding J, Richardson R, Cameron A, O'Leary S, Wallace GG, Clark GM. J. Controlled Release. 2006; 116:285.c) Richardson RT, Thompson B, Moulton S, Newbold C, Lum MG, Cameron A, Wallace G, Kapsa R, Clark G, O'Leary S. Biomaterials. 2007; 28:513. [PubMed: 17007922] d) Thompson BC, Richardson RT, Moulton SE, Evans AJ, O'Leary S, Clark GM, Wallace GG. J. Controlled Release. 2010; 141:161.e) Cui X, Hetke JF, Wiler JA, Anderson DJ, Martin DC. Sens. Actuators, A. 2001; 93:8.f) Cui X, Lee VA, Raphael Y, Wiler JA, Hetke JF, Anderson DJ, Martin DC. J. Biomed. Mater. Res. 2001; 56:261. [PubMed: 11340598] g) Cui X, Martin DC. Sens. Actuators, B. 2003; 89:92.h) Cui X, Wiler J, Dzaman M, Altschuler RA, Martin DC. Biomaterials. 2003; 24:777. [PubMed: 12485796] i) Cui XT, Zhou DD. IEEE Trans. Neural Syst. Rehabil. Eng. 2007; 15:502. [PubMed: 18198707] j) Stauffer WR, Cui XT. Biomaterials. 2006; 27:2405. [PubMed: 16343612] k) Wadhwa R, Lagenaur CF, Cui XT. J. Controlled Release. 2006; 110:531.l) Cui XY, Hetke JF, Wiler JA, Anderson DJ, Martin DC. Sens. Actuators, A. 2001; 93:8.m) Cui XY, Martin DC. Sens. Actuators, B. 2003; 89:92.n) Cui X, Wiler J, Dzaman M, Altschuler RA, Martin DC. Biomaterials. 2003; 24:777. [PubMed: 12485796] o) Cui XT, Zhou DD. IEEE Trans. Neural Syst. Rehabil. Eng. 2007; 15:502. [PubMed: 18198707] p) Wadhwa R, Lagenaur CF, Cui XT. J. Controlled Release. 2006; 110:531.q) Green R, Abidian MR. Adv. Mater. 2015; 27:7620. [PubMed: 26414302]
10. Paul N, Muller M, Paul A, Guenther E, Lauermann I, Muller-Buschbaum P, Lux-Steiner MC. Soft Matter. 2013; 9:1364.
11. a) Pernaut JM, Reynolds JR. J. Phys. Chem. B. 2000; 104:4080.b) Miller LL, Zhou XU. Macromolecules. 1987; 20:1594.c) Kontturi K, Pentti P, Sundholm G. J. Electroanal. Chem. 1998; 453:231.d) Massoumi B, Entezami AA. Polym. Int. 2002; 51:555.e) Leprince L, Dogimont A, Magnin D, Demoustier-Champagne S. J. Mater. Sci. Mater. Med. 2010; 21:925. [PubMed: 20143134] f) Alba N, Du Z, Catt K, Kozai T, Cui X. Biosensors. 2015; 5:618. [PubMed: 26473938]
12. Stauffer WR, Lau PM, Bi GQ, Cui XT. J. Neural Eng. 2011; 8:044001. [PubMed: 21633143]
13. a) Ben-Ari Y, Khazipov R, Leinekugel X, Caillard O, Gaiarsa J-L. Trends Neurosci. 1997; 20:523. [PubMed: 9364667] b) Ruel J, Bobbin RP, Vidal D, Pujol R, Puel J-L. Neuropharmacology. 2000; 39:1959. [PubMed: 10963740]

14. a) Lee SH, Govindaiah G, Cox CL. J. Neurophysiol. 2010; 103:1728. [PubMed: 20107128] b) Dalia A, Uretsky NJ, Wallace LJ. Brain Res. 1996; 728:209. [PubMed: 8864484] c) Martin A, Recasens M, Guiramand J. Neurochem. Int. 2003; 42:251. [PubMed: 12427479]
15. a) Lu Y, Li T, Zhao X, Li M, Cao Y, Yang H, Duan YY. Biomaterials. 2010; 31:5169. [PubMed: 20382421] b) Chen GZ, Shaffer MS, Coleby D, Dixon G, Zhou W, Fray DJ, Windle AH. Adv. Mater. 2000; 12:522.c) Lee Y-K, Lee K-J, Kim D-S, Lee D-J, Kim J-Y. Synth. Metals. 2010; 160:814.d) Luo X, Matranga C, Tan S, Alba N, Cui XT. Biomaterials. 2011; 32:6316. [PubMed: 21636128]
16. Kolarcik CL, Catt K, Rost E, Albrecht IN, Bourbeau D, Du Z, Kozai TD, Luo X, Weber DJ, Tracy Cui X. J. Neural Eng. 2015; 12:016008. [PubMed: 25485675]
17. a) Zou J, Tran B, Huo Q, Zhai L. Soft Mater. 2009; 7:355.b) Bhandari S, Deepa M, Srivastava AK, Joshi AG, Kant R. J. Phys. Chem. B. 2009; 113:9416. [PubMed: 19545156] c) Luo X, Weaver CL, Zhou DD, Greenberg R, Cui XT. Biomaterials. 2011; 32:5551. [PubMed: 21601278]
18. Pyo M, Reynolds JR. Chem. Mater. 1996; 8:128.
19. Ahissar E, Sosnik R, Haidarliu S. Nature. 2000; 406:302. [PubMed: 10917531]
20. Williams JC, Hippensteel JA, Dilgen J, Shain W, Kipke DR. J. Neural Eng. 2007; 4:410. [PubMed: 18057508]
21. Abidian MR, Kim DH, Martin DC. Adv. Mater. 2006; 18:405. [PubMed: 21552389]
22. Rose TL, Robblee LS. IEEE Trans. Biomed. Eng. 1990; 37:1118. [PubMed: 2276759]
23. Shannon RV. IEEE Trans. Biomed. Eng. 1992; 39:424. [PubMed: 1592409]
24. a) Wagenaar DA, Pine J, Potter SM. J. Neurosci. Methods. 2004; 138:27. [PubMed: 15325108] b) Wagenaar DA, Potter SM. J. Neurosci. Methods. 2002; 120:113. [PubMed: 12385761]
25. a) Simons DJ. J. Neurophysiol. 1985; 54:615. [PubMed: 4045540] b) Wang Q, Millard DC, Zheng HJ, Stanley GB. J. Neural Eng. 2012; 9:026008. [PubMed: 22327024] c) Beltramo R, D'Urso G, Dal Maschio M, Farisello P, Bovetti S, Clovis Y, Lassi G, Tucci V, De Pietri Tonelli D, Fellin T. Nat. Neurosci. 2013; 16:227. [PubMed: 23313909] d) Hooks BM, Hires SA, Zhang Y-X, Huber D, Petreanu L, Svoboda K, Shepherd GMG. PLoS Biol. 2011; 9:e1000572. [PubMed: 21245906]
26. Simons DJ, Carvell GE, Hershey AE, Bryant DP. Exp. Brain Res. 1992; 91:259. [PubMed: 1459228]
27. Hofmann L, Ebert M, Tass PA, Hauptmann C. Front. Neuroeng. 2011; 4:e00009.
28. Simon DT, Kurup S, Larsson KC, Hori R, Tybrandt K, Goiny M, Jager EW, Berggren M, Canlon B, Richter-Dahlfors A. Nat. Mater. 2009; 8:742. [PubMed: 19578335]
29. George PM, LaVan DA, Burdick JA, Chen CY, Liang E, Langer R. Adv. Mater. 2006; 18:577.

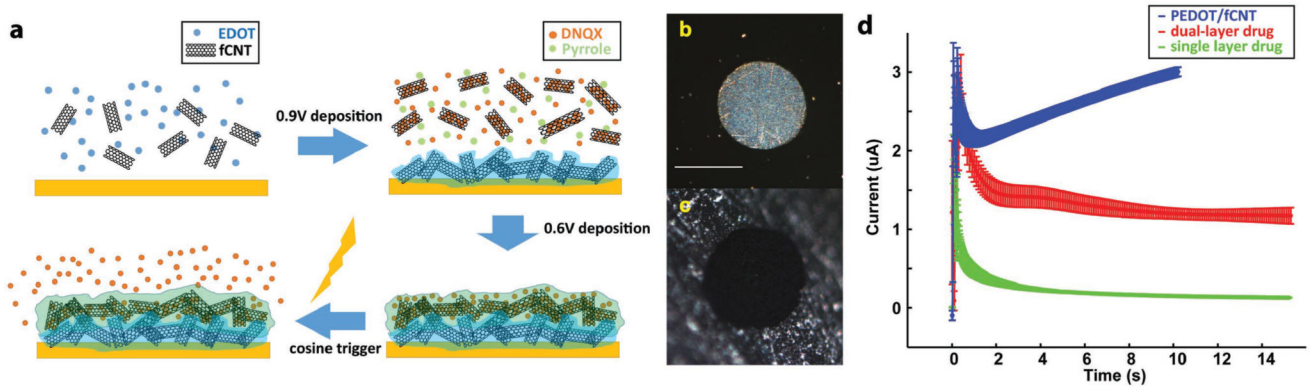

Figure 1.

a) Illustration of the synthesis of dual-layer PEDOT/fCNT-PPy/fCNT/DNQX film and controlled release of DNQX from the film; b) microscope examination of custom-built in vitro microelectrode, scale bar = 100 μm; c) picture of PEDOT/fCNT-coated in vitro microelectrode site; d) chronoamperometry deposition of PEDOT/fCNT (n = 4), dual-layer PPy/fCNT/fluorescein (n = 4), and single-layer PPy/fCNT/fluorescein (n = 3).

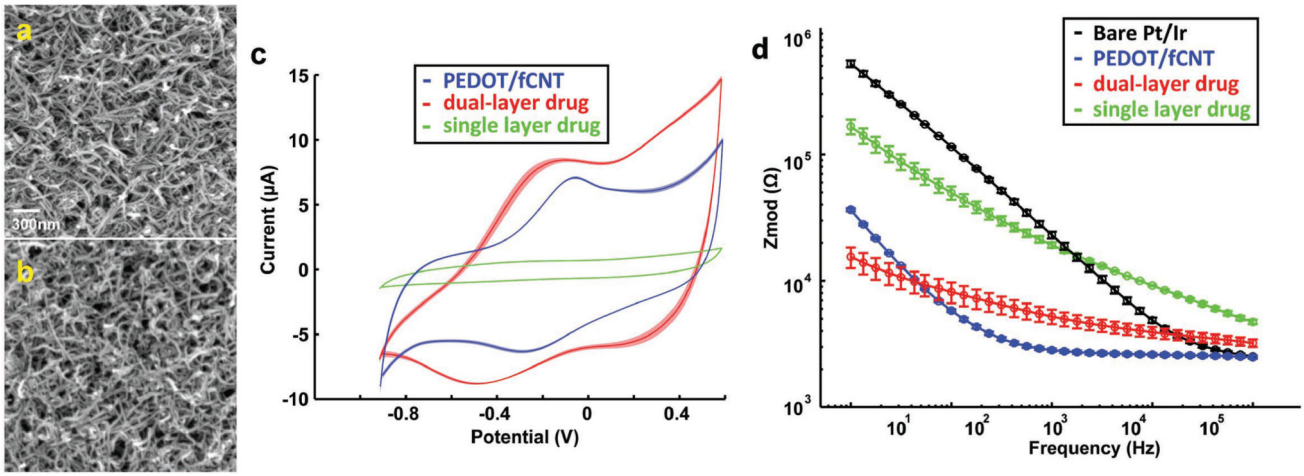

Figure 2.

a) SEM image of PEDOT/fCNT, scale bar = 300 nm; b) SEM image of dual-layer PPy/fCNT/fluorescein; c) CV of dual-layer ($n = 3$) and single-layer ($n = 3$) PPy/fCNT/fluorescein film; d) electrochemical impedance spectrum (EIS) of in vitro Pt/Ir microelectrode ($n = 5$), PEDOT/fCNT ($n = 3$), and dual-layer ($n = 3$) and single-layer ($n = 3$) PPy/fCNT/fluorescein.

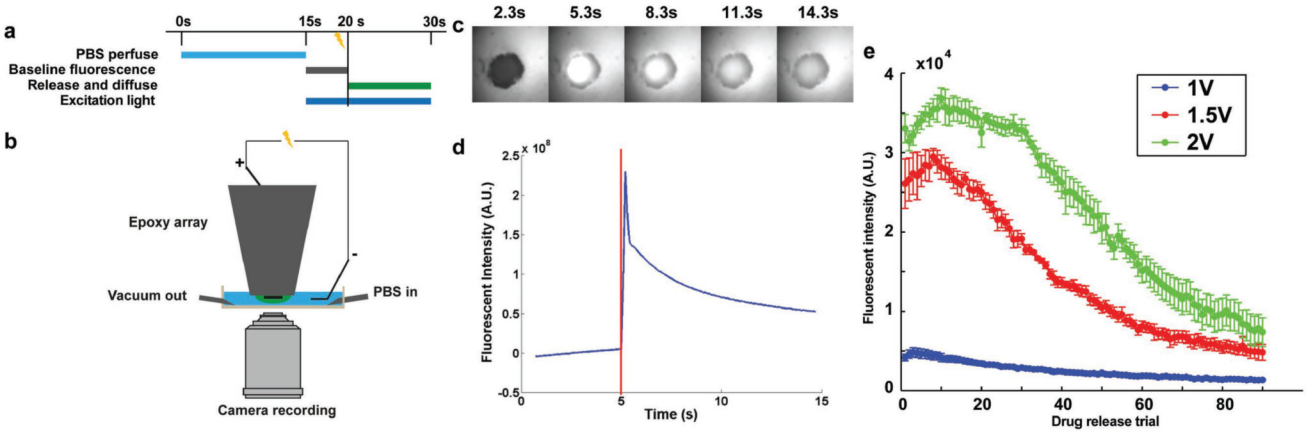

Figure 3.

a) Timing scheme of in vitro fluorescein release quantification experiment; b) microscopy semiquantification of fluorescein release setup; c) image series of representative fluorescein release from in vitro MEA, and the drug release was triggered at 5 s; d) fluorescent intensity of the electrochemically controlled release, represented by the highest fluorescent intensity subtracting the baseline intensity prior to stimulation. Vertical red line indicates onset of electrochemically controlled release waveform; e) summary of triggered fluorescence intensity increases with stimulus amplitude of 1 V ($n = 5$), 1.5 V ($n = 5$), and 2 V ($n = 6$).

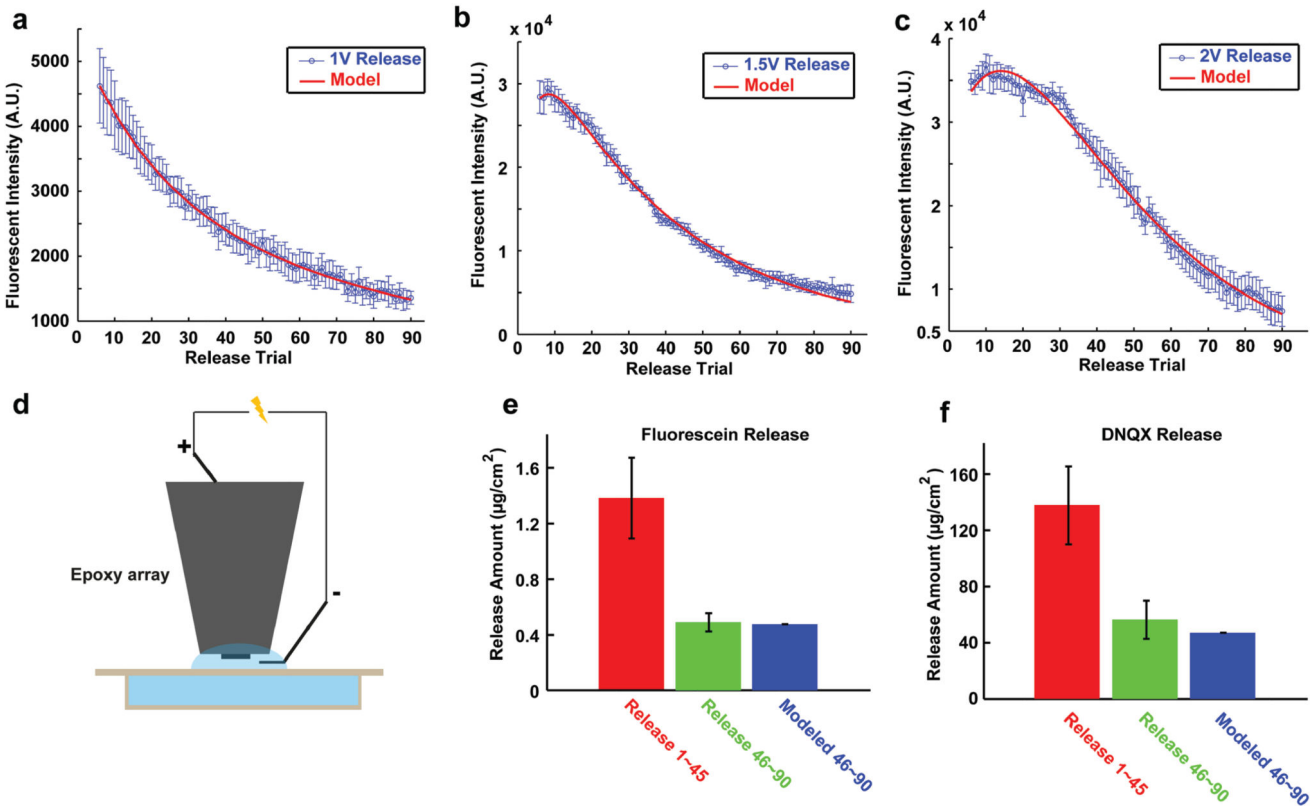

Figure 4.

a) 1 V release from in vitro microelectrode and the model fitting curve; b) 1.5 V release and model fitting curve; c) 2 V release and model fitting curve; d) spectrometry quantification setup for fluorescein and DNQX release; e) cumulated fluorescein release quantity for release trigger 1–45 and 46–90 ($n = 3$), with the model predicted release 46–90 by release volleys 1–45, and error bar is standard error of sample (SEM); f) cumulated DNQX release for trigger 1–45 and 46–90 ($n = 3$) as well as the model predicted release 46–90.

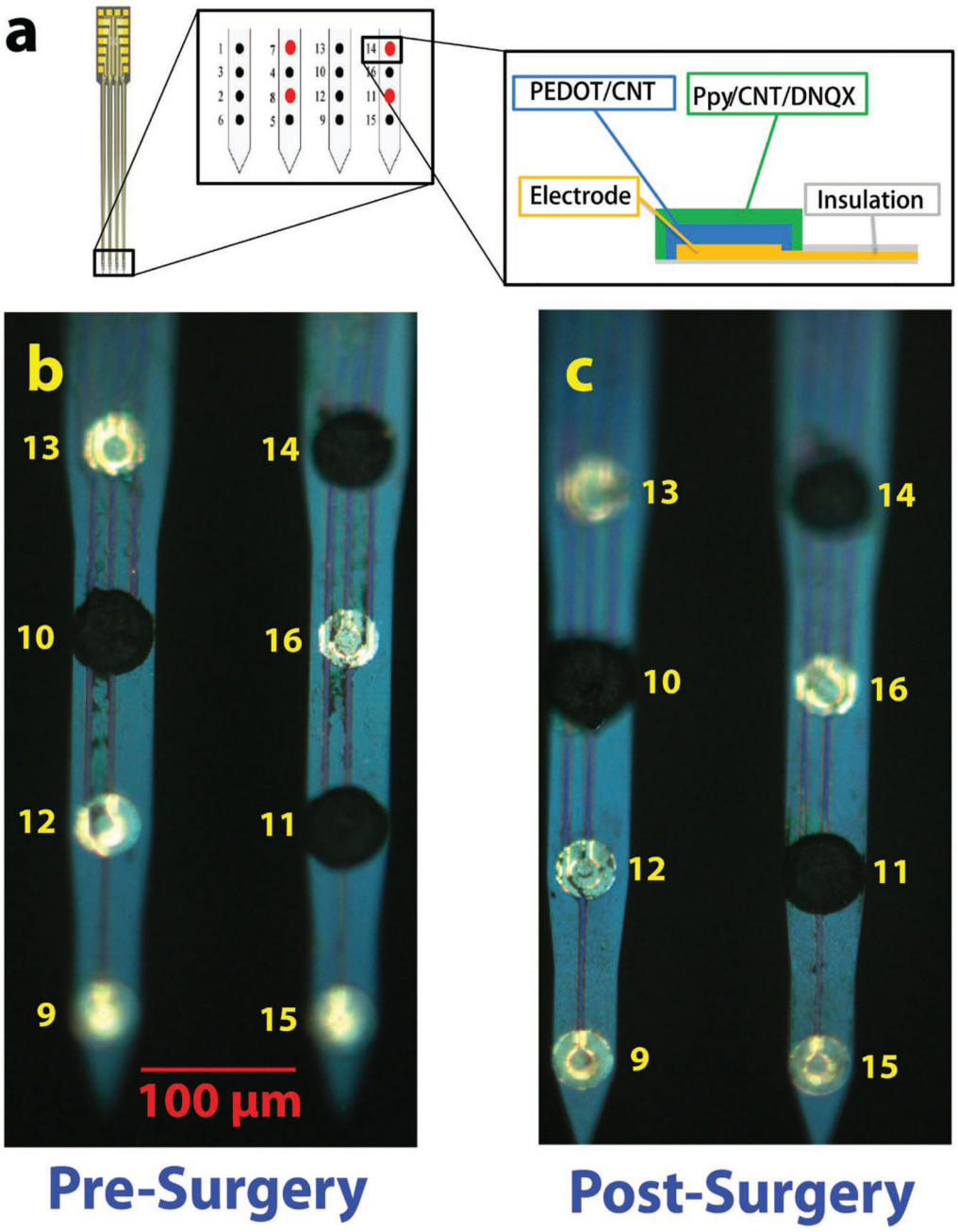

Figure 5.

a) Bilayer coating scheme on in vivo MEA, and the middle subpanel is the zoom-in demonstration of electrode sites at tip of MEA and the right subpanel is the zoom-in demonstration of bilayer drug loading film on electrode sites; b) microscopic image of the dual-layer PPy/fCNT/DNQX film compared with uncoated iridium sites; c) image of film after drug release in vivo.

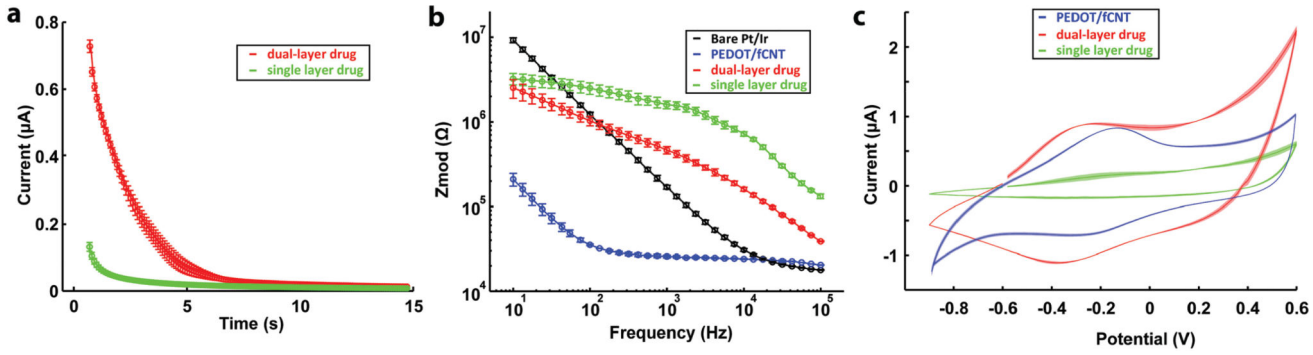

Figure 6.

a) Chronoamperometry deposition of dual-layer ($n = 3$) and single-layer ($n = 4$) PPy/fCNT/DNQX, and the semitransparent shadow denotes the standard error; b) EIS of in vivo microelectrode ($n = 3$), PEDOT/fCNT ($n = 3$), and dual-layer ($n = 3$) PPy/fCNT/DNQX; c) CV of dual-layer ($n = 3$) and single-layer ($n = 3$) PPy/fCNT/DNQX.

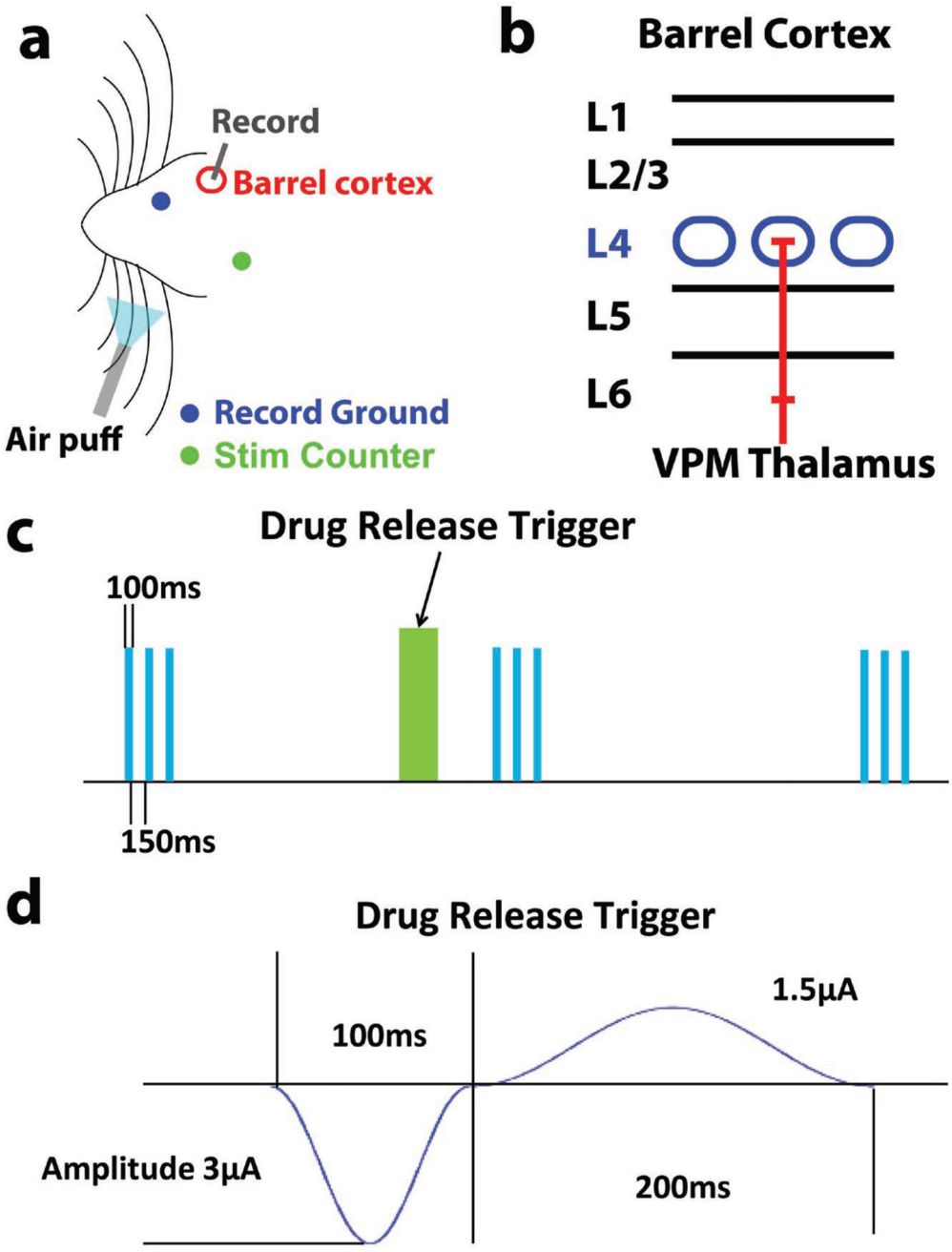

Figure 7.

a) Surgery schematics for in vivo characterization of drug release effectiveness; b) schematics for rat barrel cortex layer structure, and L4 in blue color is the target implantation depth; c) scheme of drug delivery and air puff sensory stimulation paradigm, green block is drug release, and blue block is air puff; d) in vivo drug release trigger cosine waveform.

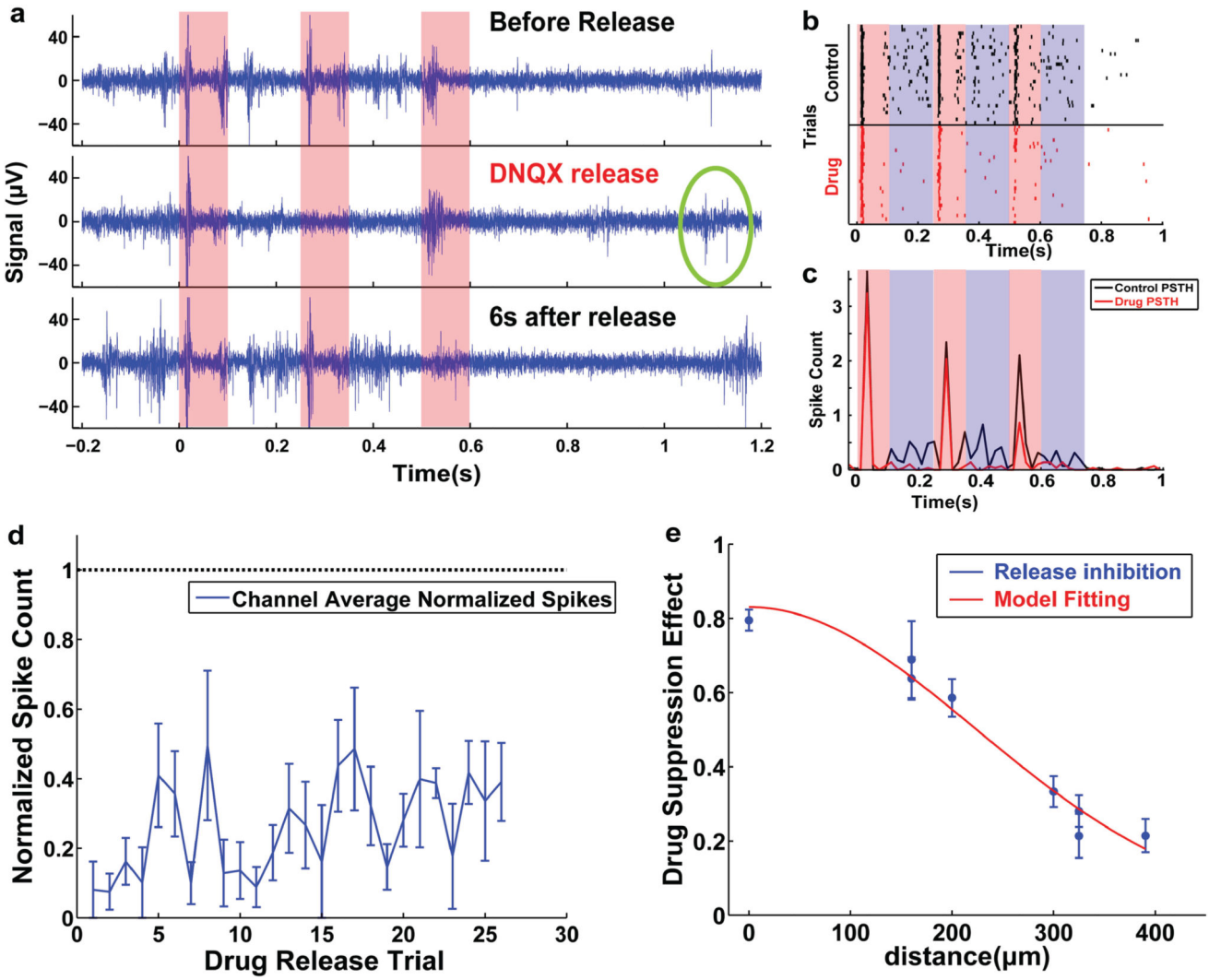

Figure 8.

a) Representative air puff evoked sensory response (upper panel) and the drug release affected action potentials (middle panel), as well as recovered neural response 6 s after release (lower panel); b) raster plot of air puff evoked spikes and drug release suppressed spikes; c) peristimulus time histogram of air puff evoked spike count and drug release suppressed activity; d) channel average of drug effectiveness over trials indicates the DNQX release suppress neural activity for at least 26 times; e) trial average of drug effectiveness indicates that the DNQX effect extends to 446 μm in vivo, and red curve indicates the Gaussian function fitting.

Table 1

Model fitting parameters for fluorescein release experiment.

Amplitude	1 V	1.5 V	2 V
A	2.93×10^3	4.08×0^4	9.57×10^5
B	−0.040	−0.026	−0.038
C	0.824	−0.564	−0.971
D	−0.007	−0.208	−0.042
R^2	0.996	0.994	0.994